12th International Conference on Fracture Mechanics of Concrete and Concrete Structures
FraMCoS-12
B.L.A. Pichler, Ch. Hellmich, P. Preinstorfer (Eds)

https://doi.org/10.21012/FC12.1192
MS17-2:4

MESO-LEVEL HPC ANALYSIS OF CONCRETE SPECIMENS SUBJECT TO EXTERNAL SULFATE ATTACK, AND COMPUTATIONAL ASPECTS

C. BISCARO[*], C.M. LÓPEZ[†], G. XOTTA[*], D.GAROLERA[††], I. CAROL[†]

[*] University of Padova, Department of Civil, Environmental and Architectural Engineering,
Via Marzolo 9, 35131 Padova, Italy
e-mail: giovanna.xotta@unipd.it

[†] Universitat Politècnica de Catalunya, Department of Civil and Environmental Engineering,
Campus Nord UPC, Jordi Girona 1, Edif D2, E-08034 Barcelona
e-mail: carlos.maria.lopez@upc.edu, ignacio.carol@upc.edu

[††] DRACSYS, S.L., Campus Nord UPC, Jordi Girona 1, Edif K2M-202E, E-08034 Barcelona
e-mail: daniel.garolera@dracsys.com

Key words: External Sulphate Attack, concrete degradation, chemo-mechanical modeling, interface element

Abstract: Concrete is considered a heterogeneous material composed of aggregates enclosed by a mortar matrix. The Finite Element analysis is performed by inserting zero-thickness interface elements in between continuum elements along pre-selected paths representing main potential crack paths. These interface elements are equipped with a fracture-based constitutive law. In previous literature this approach has been shown to provide very realistic results in the study of concrete fracture. Moreover, remeshing becomes unnecessary by the a-priori insertion of these elements where the fracture capability is concentrated, and the problem of localized deformation in the continuum elements is also overcome. However, using this approach a duplication of nodes occurs along the surfaces where they are inserted, and this may lead to a very high computational effort. In recent years, the group of Mechanics of Materials (MECMAT) at the Universitat Politècnica de Catalunya (UPC) has devoted substantial effort to extend the applicability of such approach to a variety of coupled problems, and to increase its efficiency via Message Passing Interface (MPI) parallelization and Portable, Extensible Toolkit for Scientific Computation (PETSc) libraries. In particular, these improvements have also been applied to the 3-D analysis of concrete specimens subject to External Sulphate Attack (ESA). In this context, the paper describes the coupled Chemo-Mechanical (C-M) model, presents the latest results obtained with various meshes of progressively larger sizes, and shows the scalability of the parallel implementation developed. Additionally, the paper describes a new technique developed to reduce computation times, consisting of identification of continuum blocks surrounded by interface elements and eliminating internal nodes using a Schur complement scheme. The new strategy has only been implemented so far in sequential mode, but results are presented that lead to significant reduction in computation time, and work is under way to achieve full parallel version of this technique.

1 INTRODUCTION

In recent years there has been a growing interest in determining and understanding concrete degradation processes. In particular,

when concrete is subjected to an environment characterized by high humidity and rich in sulphate ions, a degradation process due to ESA may be initiated. Sulphate penetrating into concrete activates a series of chemical reactions that lead to the formation of secondary ettringite. This process can induce non-uniform volumetric expansions that may generate cracking. In turn, cracking can further facilitate sulphate penetration. Therefore ESA may be considered a coupled chemical-mechanical problem.

In this work, the numerical analysis of ESA is conducted using the Finite Element Method, by considering the specimen at the meso-level composed of larger aggregates embedded in a mortar matrix. Standard continuum finite elements are used to discretize aggregates and mortar, while zero-thickness elements are inserted along all the aggregate-mortar and selected mortar-mortar contacts to represent potential cracks.

The diffusion-reaction of sulphate ions (chemical problem) is modelled following Tixier and Mobasher [1] and Idiart et al. [2]. Regarding the mechanical problem, continuum elements are assumed to exhibit linear elastic behaviour, while interface elements behave according to an elasto-plastic law based on fracture mechanics [3-4].

The fully parallelized in-house DRAC5 code, developed originally within the MECMAT group at UPC, and more recently by spinoff company of the group DRACSYS, is used to solve both mechanical and chemical problems through a staggered scheme. This has allowed the analysis of new and more challenging 3D studies, producing realistic results that reflect the 'onion peeling' cracking pattern, similar to what observed in laboratory [5] and 2D cases previously studied [4].

Finally, a new solution technique based on sub structuring and Schur complement, which substantially reduces the number of degrees of freedom to be considered during the iterative process, has been preliminarily implemented in DRAC4, a simpler series version of the code, and has been tested showing great advantages in terms of solution time for a number of 2D application examples.

2 CONSTITUTIVE MODEL

2.1 Meso-mechanical model

As mentioned above, in the meso-mechanical investigations for this type of problem, aggregates and cement paste are defined as continuous elements that observe an elastic mechanical behaviour. Differently, the interface elements are characterized by an elasto-plastic constitutive law that incorporates concepts of fracture mechanics and fracture energy. The features of these elements were initially designed for their use in 2D analyses and subsequently expanded to encompass 3D analyses [3-4,6]. The formulation of the interface elements is expressed in relation to the normal and shear components of the stresses at the interface plane, denoted as $\boldsymbol{\sigma}_J = [\sigma_N, \tau_1, \tau_2]^T$. Additionally, a corresponding set of relative displacements, identified as crack opening/sliding, is represented by the vector $\boldsymbol{r} = [r_N, r_{T1}, r_{T2}]^T$.

A three-parameter hyperbola is used to define the loading (plasticity) function:

$$F(\boldsymbol{\sigma}) = -(c - \sigma_N \tan\phi) + \sqrt{\tau^2 + (c - \chi tan\phi)^2} \quad (1)$$

where τ represents the modulus of the shear stresses present at the interface plane (i.e. $\tau = \sqrt{\tau_1^2 + \tau_2^2}$), while the variable χ is used to denote the tensile strength, which corresponds to the normal stress at the vertex of the hyperbola. Additionally, the symbol c represents the apparent cohesion, while $\tan\phi$ is used to represent the internal friction angle.

When the stress state on the surface reaches $F(\boldsymbol{\sigma}) = 0$ and cracking begins, the loading surface begins to contract as the primary parameters decrease in accordance with the evolution laws that are based on the work that is dissipated in the fracture process (W^{cr}).

The hyperbolic fracture surface facilitates a seamless and continuous transition between the two extreme loading scenarios, namely the conventional tensile fracture mode and the mode involving shear and very high compression. In order to regulate and manage these distinct fracture modes, the model

employs the concept of dissipated fracture energy.

2.2 Chemical transport model

The diffusion-reaction problem is described using the direct approach proposed by Tixier and Mobasher, later refined by Idiart et al. [1-2]. The external sulphate attack phenomenon is assumed to be contingent upon the concentration of a solitary diffusing species, specifically the sulphate ions, which constitutes the main variable of the reactive transport model. Upon first contact with concrete, sulphate reacts with portlandite (CH) to produce gypsum. Subsequently, the resulting gypsum may interact with any of the four distinct phases of calcium aluminate ($C_4AH_{13}, C_4A\bar{S}H_{12}, C_3A$ and C_4AF), thereby resulting in the generation of secondary ettringite ($C_6A\bar{S}_3H_{32}$).

Since there is little information on individual kinetics, the four reactions leading to the formation of secondary ettringite are here grouped into a single expression given by:

$$C + qU \longrightarrow C_6A\bar{S}_3H_{32} \tag{2}$$

where the equivalent aluminate concentration (mol/m^3) $C = \gamma_1 C_4AH_{13} + \gamma_2 C_4A\bar{S}H_{12} + \gamma_3 C_3A + \gamma_4 C_4$ and the stoichiometric weighted coefficient $q = 3\gamma_1 + 2\gamma_2 + 3\gamma_3 + 4\gamma_4$ of the sulphate concentration U (mol/m^3), depend on coefficients $\gamma_i = C_i / \sum C_j$ where C_i are the aluminate concentrations of each phase.

Reaction (2) occurs according to the availability of calcium sulphates and aluminates, which is assumed to be governed in time and space by a second order diffusion-reaction differential equation for the sulphate concentration (U (mol/m^3)), plus a local equation for the decrease of calcium aluminates:

$$\begin{aligned} \frac{\partial U}{\partial t} &= \frac{\partial}{\partial x}\left(D_U \frac{\partial U}{\partial x}\right) - kUC \\ \frac{\partial C}{\partial t} &= -k\frac{UC}{q} \end{aligned} \tag{3}$$

where D_U (m^2/s) denotes the diffusion coefficient of these ions through the porous medium, C (mol/m^3) indicates the amount of equivalent calcium aluminate, whereas k (m^3/mol s) identifies the combined rate of the sulfate reaction.

Sulphate ion diffusion could occur within the cement matrix and along the fracture lines. In the matrix, this phenomenon is related to the porosity of the material. Initially, higher porosity leads to a correspondingly higher rate of diffusion. However, there may be a later phase in which diffusivity decreases as the material product of the chemical reaction progressively fills the pores within the matrix.

The rate of diffusivity along the fracture lines, which are represented within the finite element mesh by means of zero-thickness interface elements, depends on the extent to which the fracture is open. With the progression of sulphate attack, the diffusivity may increase for those fracture lines that evolve into open cracks, as diffusivity in the bulk pores concurrently decreases. The value of diffusivity is expressed through a power function that depends on the crack opening [2].

It is assumed that the volumetric expansion of the solid material, ε_v, will be directly proportional to the amount of calcium aluminate that has undergone the reactive process. This amount can be determined by calculating the difference between the initial concentration CA_0 and the concentration that persists unreacted at a specific instant:

$$\varepsilon_v(t) = \alpha_s \cdot (CA_0 - C) - f \cdot \Phi_{ini} \tag{4}$$

Equation (4) includes the symbol Φ_{ini} to represent the initial capillary porosity of the material, while the variable f indicates the proportion of the initial porosity that must be saturated by precipitates before any material expansion can occur (f=0.05÷0.40). Lastly, the parameter α_s describes the mean volumetric expansion of the solid material per unit molar concentration of reacted aluminates, and can be expressed as follows:

$$\alpha_s = m^{ettr} - m^{CA} - q \cdot m^{gypsum} \quad (5)$$

here, m^{ettr}, m^{CA} and m^{gypsum} refer to the average molar volumes of ettringite, aluminates, and gypsum, respectively (m^3/mol)

3 CALCULATION STRATEGY AND CODE PARALLELIZATION

ESA is a coupled C-M process that can significantly accelerate the degradation of concrete. By inducing the formation of cracks within the material, ESA can increase the overall diffusivity of concrete, which, in turn, can exacerbate the penetration of sulphate ions and lead to further expansion and increased propensity to crack. Consequently, ESA can give rise to various phenomena, including but not limited to concrete failure and spalling, much earlier than would occur in the absence of crack-induced effects. A staggered strategy method is here employed to couple the numerical analysis of the mechanical and chemical processes. This approach involves linking two distinct calculations, so that the results of chemical problem can be utilized as input for the mechanical analysis, and the resulting outputs can then be used as input for the chemical analysis. This process is iterated until a predefined tolerance is achieved.

In the initial phases, two distinct computational codes were employed to address this problem. The chemical aspect of the problem was handled by the DRACFLOW code, which operated solely in serial mode. Conversely, the mechanical component of the problem was addressed using the DRAC code, which worked in parallel mode. Given the need to deal with increasingly complex problems, these codes have undergone modifications and enhancements [7]. Notably, the current release of the codes includes a parallel-solving code for the chemical aspect of the problem. As a result, significant MPI parallelization has been achieved for simultaneous mechanical and chemical problem solving. Moreover, the incorporation of the PETSc library has brought significant improvements, particularly in its ability to facilitate the resolution of large-scale projects.

With these improvements, it has become feasible to tackle increasingly complex problems that were previously beyond the scope of the codes. Specifically, the previous limit of addressing problems involving 50,000 nodes with a maximum of 12 CPUs, exclusively for the mechanical problem-solving aspect, has been significantly exceeded. At present, the improved codes can handle problems involving up to 400,000 nodes and use up to 72 CPUs (limitation due to the machine used).

The largest mesh analysed comprises a set of approximately 8x8x3 aggregates. Additionally, a steel plate is also represented on top of this specimen for the purpose of enforcing uniform deformations, while still allowing vertical expansions. This plate is connected to the specimen via a layer of interface elements. This mesh, as depicted in Figure 1, encompasses a grand total of 402.510 nodes, 155.302 continuum elements and 214.495 interface elements.

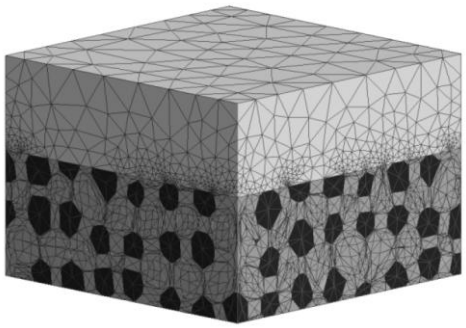

Figure 1: Mesh of 8x8x3 aggregates (402.510 nodes).

The study of the time required for the first step considered as linear for both mechanical and chemical behaviour, for one staggered iteration and for the mesh consisting of 402.510 nodes, is depicted in Figure 2. Three distinct curves are displayed: one representing the time for the chemical problem in grey, another showing the time for the mechanical problem in yellow, and the third reporting the total analysis time in blue.

It is evident that, in this scenario, for the mechanical part and thereby for the total analysis, there is a substantial reduction in time when going from 2 to 16 CPUs. Thereafter, the

time reaches its minimum value at 32 CPUs, and then rises once more with the use of 64 CPUs. The reduction can be attributed to the fragmentation of RAM across multiple processors, and thus each processor individually handles a smaller portion of the problem. However, an optimal value, that can be uniquely defined for each specific problem, is reached at 32 CPUs, which minimises computation time. Beyond this optimal threshold, as the number of CPUs increases further, an inverse effect becomes evident. Excessive fragmentation of the problem leads to an increase in the time required for its resolution.

All analyses were executed on the group's dedicated server, a DELL Poweredge 6525, equipped with a single node containing 2x64-core AMD EPYC 7662 processors and 1 terabyte of RAM.

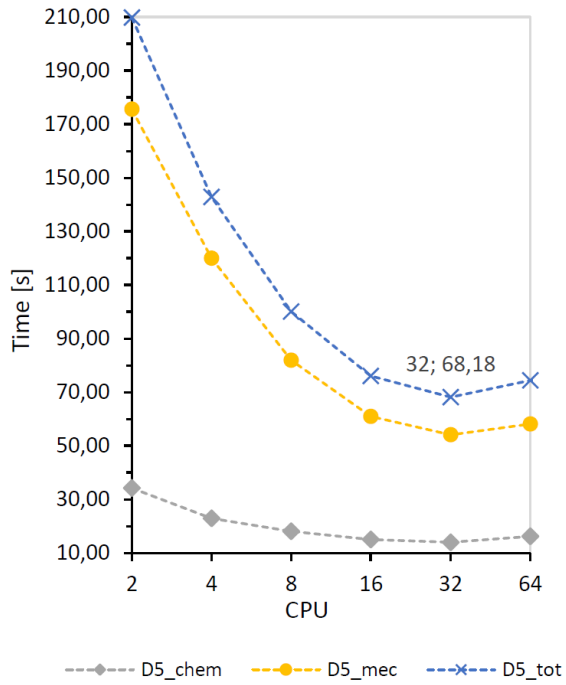

Figure 2: Time required to solve the problem of the mesh with 402.510 nodes.

4 3D ESA NUMERICAL EXAMPLES

The improved and more robust implementation of the code has enabled the analysis of larger and more complex 3D problems that were previously unattainable. In this regard, we present the results of a study conducted on two specimens of different sizes in the plane while maintaining a constant height, 6x6x4 cm^3 and 10x10x4 cm^3, both featuring the same aggregate/matrix ratio.

The geometry of the two concrete specimens consists of 75 (5x5x3) and 192 (8x8x3) aggregate particles embedded in a mortar matrix. Instead, their discretization, depicted in Figure 3, is carried out using respectively 52.297 and 142.360 tetrahedral continuum elements, 77.313 and 211.019 triangular interface elements, for a total of 147.189 and 398.956 nodes.

A minimum number of kinematic constraints is applied to the two meshes, to prevent rigid rotations, and they are subjected to sulphate attack on all four side faces (samples are considered immersed in a solution with a sulphate concentration of 35,2 mol/m^3).

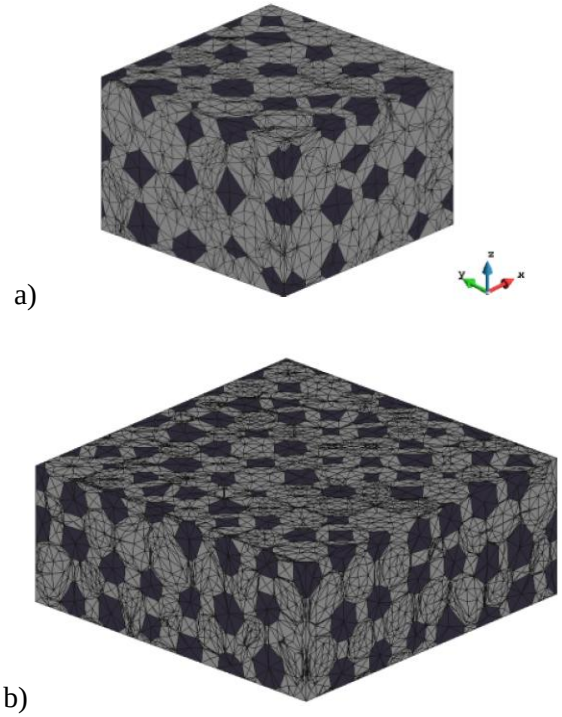

Figure 3: Characteristics of the two 3D meshes: a) 6x6x4 cm^3 specimen; b) 10x10x4 cm^3 specimen.

Figures 4 and 5 illustrate the progression of sulphate and ettringite (with a top and side view; aggregates have been omitted to improve visibility of penetration fronts) and deformation (of a mid-plane section), at 2000 and 4000 days after sulphate attack, for the 6x6x4 cm^3 and 10x10x4 cm^3 specimens, respectively.

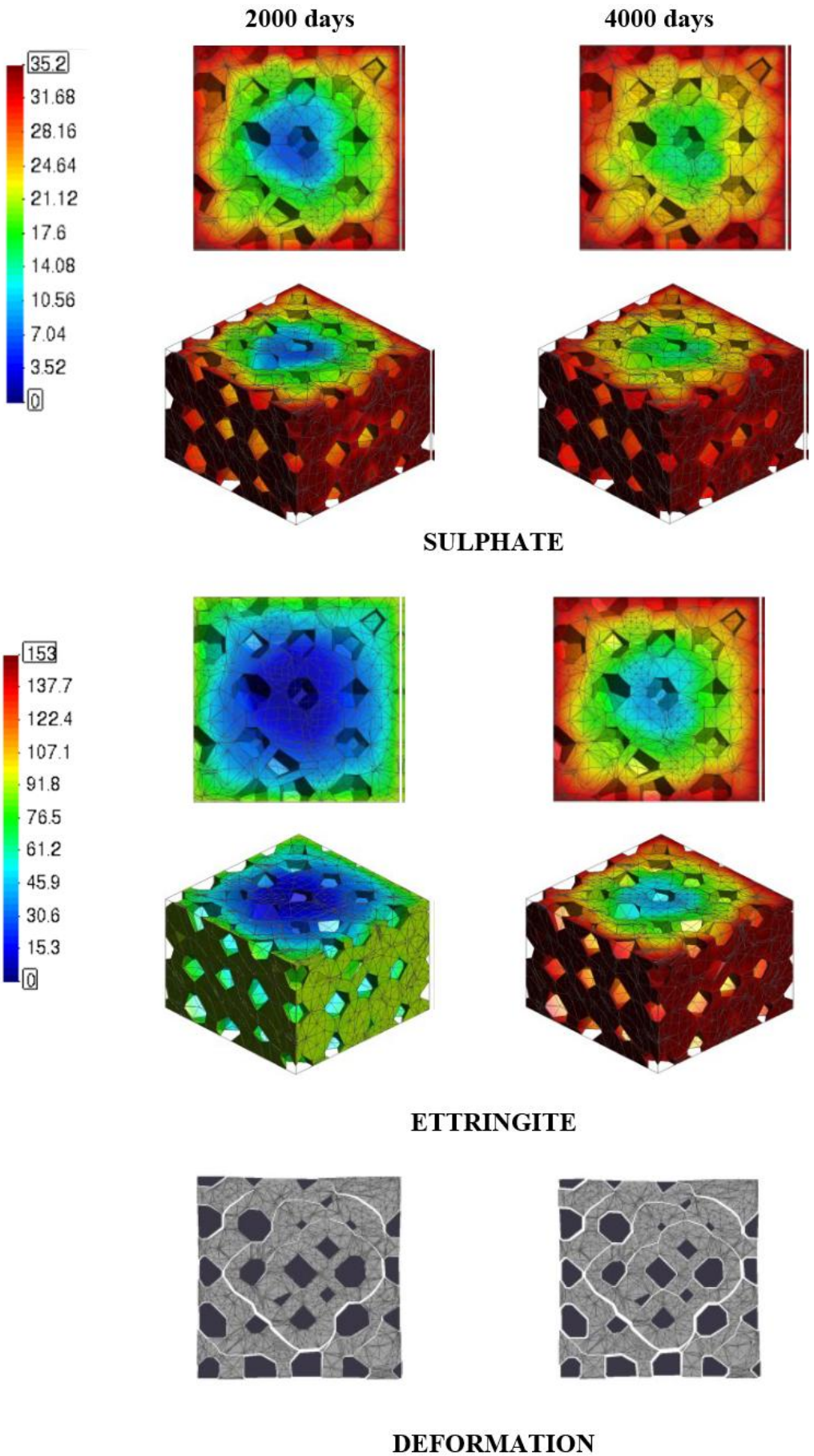

Figure 4: Sulphate concentration [mol/m^3], ettringite [kg/m^3] progression and deformation for the 6x6x4 cm^3 specimen.

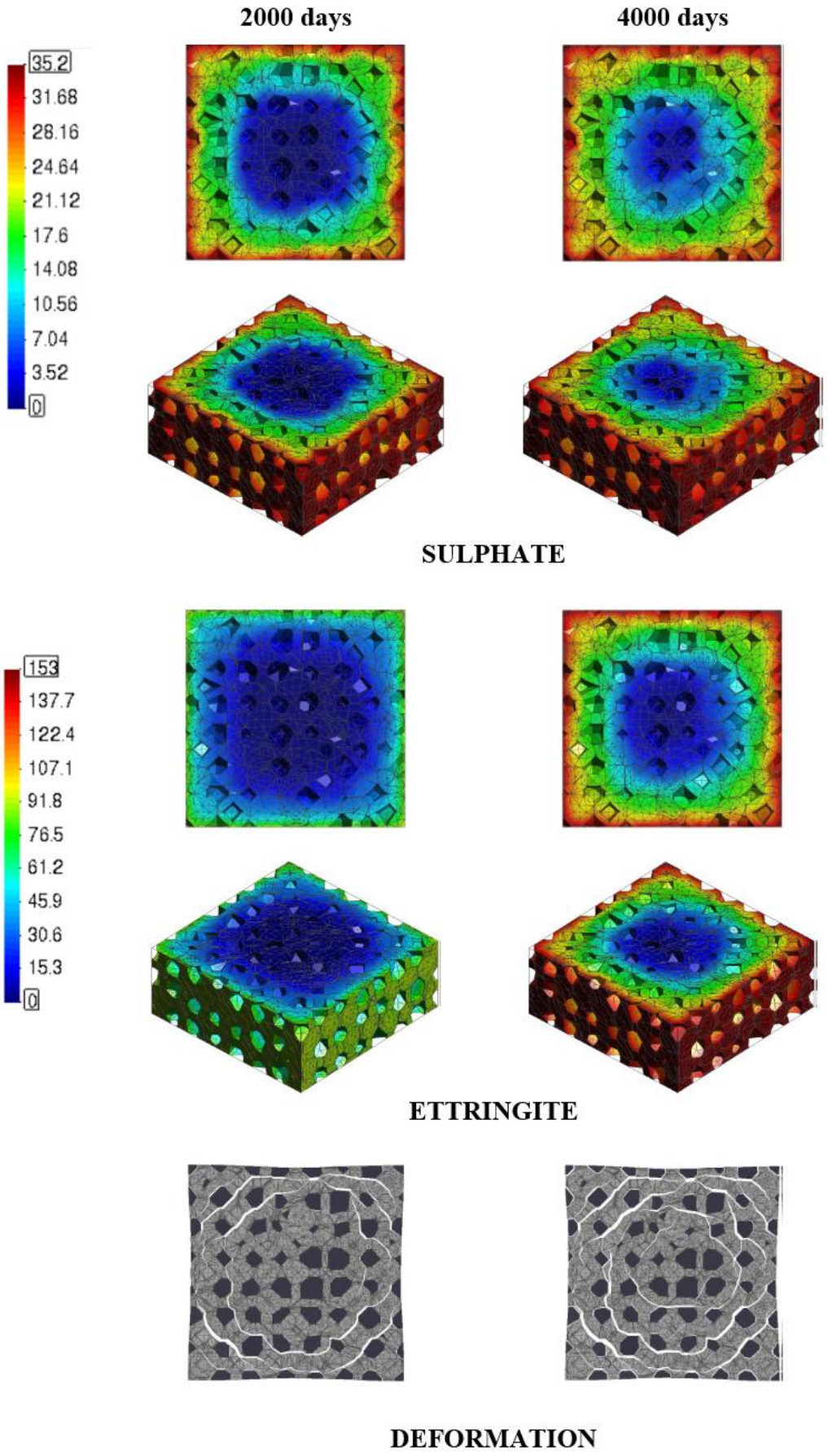

Figure 5: Sulphate concentration [mol/m^3], ettringite [kg/m^3] progression and deformation for the 10x10x4 cm^3 specimen.

In both figures, a gradual advancement of the sulphate concentration front towards the interior of the specimen is illustrated; this phenomenon is a result of a coupled problem arising from the expansion process that generates fractures and the high transmissivity of the open joints, leading to a rapid and progressive penetration of the sulphate front. Additionally, the formation of ettringite increases and gradually propagates inward into the sample. However, the propagation of the ettringite front is delayed compared with that of the sulphate front because of the limited reaction rate**.**

As regarding deformations, on the other hand, considering specimens of different sizes but sharing an identical aggregate size and aggregate/matrix ratio, it becomes evident that the size exerts a discernible influence on the nature of the fractures formed. In the smaller specimen, a distinct fracture ring becomes discernible, emerging after 2000 days. The deformation pattern in this case remains fairly constant, intensifying as the formation of ettringite progresses. Conversely, in the larger specimen hosting an increasing number of aggregates, a more intricate structural response is observed. This larger sample exhibits the characteristic onion peel fracture, characterised by the development of four distinct fracture sections. This fracture pattern signifies the interplay of factors such as specimen size and aggregate distribution.

Notably, this fully coupled external chemo-mechanical sulphate attack model, proves to be instrumental in capturing cracks that evolve within the specimen. These cracks are not solely attributed to the direct presence of ettringite at specific points but also result from the expansion transmitted between interface elements distributed throughout the mesh.

4 NEW STRATEGY TO IMPROVE EFFICIENCY WITH ZERO-THICKNESS INTERFACE ELEMENTS

According to the considerations in the previous sections, the numerical model used to represent concrete at the meso-level assumes elastic behaviour for aggregates and cement matrix, while interface elements, pre-inserted along all potential crack trajectories, are regarded as non-linear and thus concentrate the capability of representing cracking and fracture. This leads to the duplication of nodes along the surfaces where they are inserted, or multiplication by 4 or even 8 or more at the points of intersection of two or more interface elements. Furthermore, investigating external sulphate attack with 3D specimens demands substantial computational resources, primarily due to the unpredictability of crack paths. To effectively capture the various potential fractures, a significant number of interface elements must be included. This makes the analysis particularly demanding from the outset, even though many interface elements may not be activated immediately or might never be involved in the fracture process.

Hence the motivation about the need to formulate an innovative methodology to address large-scale problems with a high number of interface elements.

The proposed approach takes advantage of the distinctive features of the interface elements, which are the only elements in which the non-linearity of the problem is concentrated. This makes it possible to partition the overall system of equations in two parts; a first part linear and constant, consisting of the contributions by the elements of the continuum, and a second part that may change during the iterative process and comes from the contribution of the interfaces. Then the first part can be eliminated upfront of the solution of the non-linear problem by using the so-called Schur complement, which may reduce substantially the size of the system to be solved repeatedly during the iterations of the non-linear problem. The gains of this strategy, at the moment seamlessly integrated into a series version of the code, DRAC4, are shown for some basic 2D examples.

The analysis focuses on three 2D square meshes, each containing an increasing number of continuum elements. The first is 64x64, with a total of 4.096 continuum elements, the second is 128x128, with a total of 16.384 continuum elements, and the third is 256x256, with a total

of 65.536 continuum elements.

Within each mesh, a variable number of interface elements are strategically distributed. Specifically, they are arranged both vertically and horizontally, effectively dividing the mesh into an increasing number of smaller blocks of continuum elements surrounded by interfaces (see some examples in Figure 6).

The graph depicted in Figure 7 presents the time ratios obtained from the non-linear analysis for the different meshes divided into their corresponding block numbers; it also features a red control line aligned with an abscissa value of 1.

a)

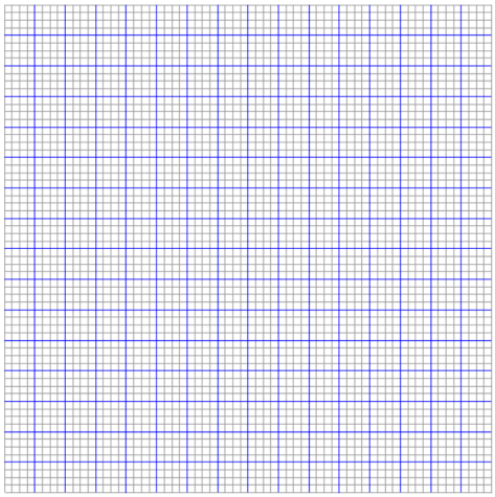

b)

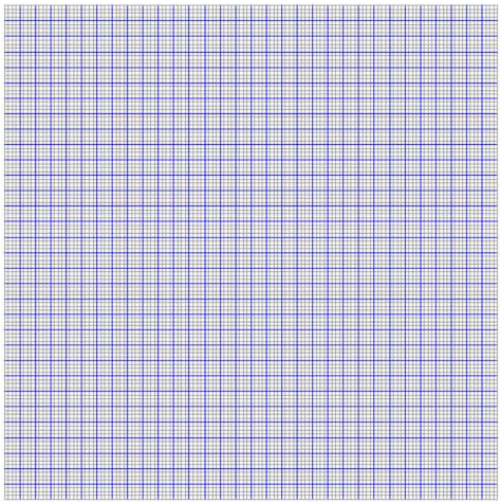

c)

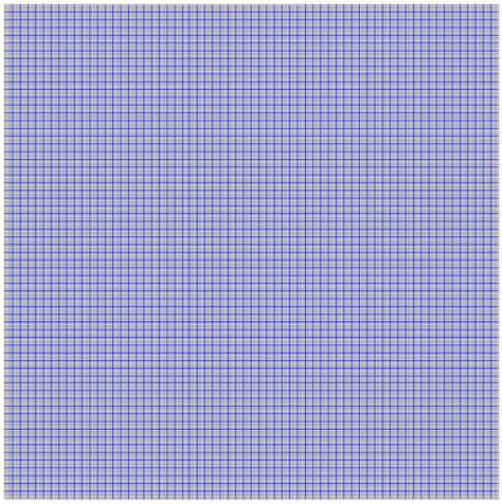

Figure 6: Examples of subdivisions in blocks for the three meshes: a) 256 blocks, 64x64 continuum elements; b) 1024 blocks, 128x128 continuum elements; c) 4096 blocks, 256x256 continuum elements.

A consistent and significant reduction in the time required for the non-linear analysis, with the new calculation scheme compared to the old one, can be obtained. In non-linear analyses, the problem must be solved repeatedly until convergence is achieved; unlike linear analyses, where one iteration is sufficient, non-linear scenarios require multiple iterations to stabilise the solution. With the new scheme, the system of the iterative process is exclusively solved for nodes of the interface, resulting in a substantial time reduction as the mesh size increases. In addition, the increase in the number of blocks leads to a decrease in time, except in the larger mesh of 256x256 elements, in which after an initial decrease the computation time seems to stabilize. This is difficult to interpret and may be the result of peculiarities of the machine architecture or memory management by the compiler or OS. To clarify these aspects, new calculations would be needed with different number of elements and blocks, different compilers or different machines.

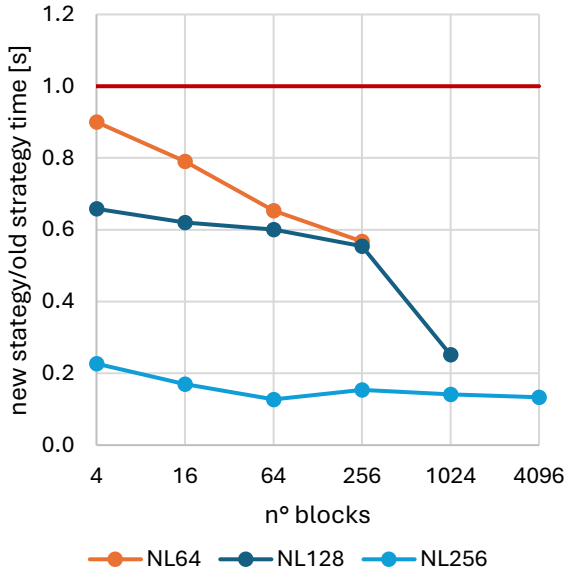

Figure 7: Ratio of new to old code time in the case of non-linear analysis.

6 CONCLUSIONS

An extensive evaluation of the updated code has been conducted, revealing good scalability and remarkable computational efficiency. The recent development of a more advanced and robust parallel implementation of the entire code has enabled even larger 3D problems to be analyzed.

The efficacy of the model employed in this study is evidenced by its capacity to accurately capture the intricate 3D degradation behaviour of concrete during external sulphate attack (ESA).

The outcomes of the simulation are in excellent agreement with the experimental observations, underscoring the realism and reliability of the model employed in this investigation (see Figure 8).

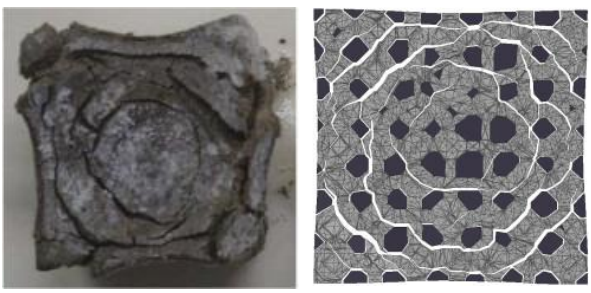

Figure 8: Experimental (Lee et al. [8]) vs. numerical spalling in a cubic specimen of concrete exposed to sulphate attack.

ACKNOWLEDGEMENTS

This research was supported by grants BIA2016–76543-R from MEC (Madrid), which includes FEDER funds, PID2020–117933 RB–100 from MCI (Madrid) and 2021SGR-00610 from AGAUR-Generalitat de Catalunya (Barcelona).

The authors C. Biscaro and G. Xotta gratefully acknowledge the financial support from the Italian Ministry of University and Research (MUR), in the framework of PRIN2020 #20209F3A37 Project.

REFERENCES

[1] Tixier, R. and Mobasher, B., 2003. Modeling of damage in cement-based materials subjected to external sulphate attack. I: Formulation. II: Comparison with experiments. *ASCE J. Mat. Civil Engng.* **15**:305-322.

[2] Idiart, A., López, C.M. and Carol, I., 2011. Chemo-mechanical analysis of concrete cracking and degradation due to sulphate attack: a meso-scale model. *Cem. Concr. Compos*. **33:**411-423.

[3] Carol, I., Prat, P.C. and López, C.M., 1997. Normal/shear cracking model: application to discrete crack analysis. *J. Eng. Mech.* **123**:765-773.

[4] Caballero, A., Carol, I. and López, C.M., 2006. A meso-level approach to the 3D numerical analysis of crackimg and fracture of concrete materials. *Fatigue Fract. Eng. Mater. Struct*. **20**:979-91.

[5] Lee, S., Hooton, R., Jung, H., Park, D., Choi, C., 2008. Effect of limestone filler on the deterioration of mortars and pastes exposed to sulfate solutions at ambient temperature. *Cem. Concr. Res*., **38**:68-76.

[6] Caballero, A., Willam, K., and Carol, I., 2008. Consistent tangent formulation for 3D interface modeling of cracking/fracture in quasi-brittle materials. *Comp. Meth. Appl. Mech. Engrg*. **197**:2804–2822.

[7] Garolera, D., 2017, Zero-thickness interface elements in petroleum geomechanics: sand production and hydraulic fracture, *Dr. Thesis*, UPC.

[8] Lee, S., Hooton, R., Jung, H., Park, D.,

Choi, C., 2008. Effect of limestone filler on the deterioration of mortars and pastes exposed to sulfate solutions at ambient temperature. *Cem. Concr. Res.*, **38**:68-76.